Authors' Camera Ready Manuscript. To appear in the
Proceedings of the 21st European Control Conference, Bucharest, Romania, Jun 2023,
Please cite using bibliographic data of the associated published version.

Cooperative control of multi-agent negative imaginary systems with applications to UAVs, including hardware implementation results

Yu-Hsiang Su, Parijat Bhowmick, *Member, IEEE*, and Alexander Lanzon, *Senior Member, IEEE*

***Abstract*— This paper proposes a new formation tracking and containment control methodology for multi-agent systems using Negative Imaginary (NI) systems theory. The proposed control scheme consists of a two-loop configuration in which the inner loop applies an appropriate feedback linearising control law to transform the nonlinear dynamics of each agent into a double integrator system, while the outer loop deploys an NI-based formation tracking and containment control protocol on the linearised double integrator agents. This methodology utilises the characteristic loci technique rather than the well-known Lyapunov-based approaches to establish the asymptotic convergence of the formation and containment trajectory tracking errors. Compared to existing methods, the proposed scheme gives more freedom to select a dynamic controller and relies only on output feedback. As a result, it offers better formation tracking and containment performance and advantages when full-state measurements are unavailable. Finally, a real-time flight experiment was conducted on networked Crazyflie quadcopters to examine the control performance in both healthy and faulty (e.g. a sudden loss of agents, communication failure, hardware faults, etc.) operating conditions.**

I. Introduction

Negative Imaginary (NI) systems theory was introduced in 2007-08 [1] and gradually flourished as a stand-alone robust control framework which parallels passivity and small-gain frameworks. At its inception, vibration control of lightly damped mechanical systems (e.g. cantilever beam) and highly resonant flexible structures [1]–[4], vibration isolator in flexible spacecrafts [5], etc., were the primary application domain of the NI theory. Later NI theory contributed to various other control and robotics application areas, especially to cooperative control of networked multi-agent systems [6] with promising applications like control of networked two-wheeled mobile robots [7]–[9], UAVs [10], train platoons [11], etc. A recent important theoretical advancement of NI theory includes dissipative characterisation of Input and/or Output NI systems [12]–[15].

Cooperative control of multi-agent systems (MAS) encompasses leader-following consensus, formation tracking, containment control, etc., and has been a promising research field over the last two decades [16]. Pioneering research on formation and containment control schemes for first-order and second-order MAS was developed in [17] and [18]. Since then, several contributions have been made in this domain. Until very recently, NI theory has been applied as an alternative approach to control MAS, such as in [6]–[10]. However, these previous MAS works based on NI theory only considered networked agents with a single role (i.e. same behaviour for all agents).

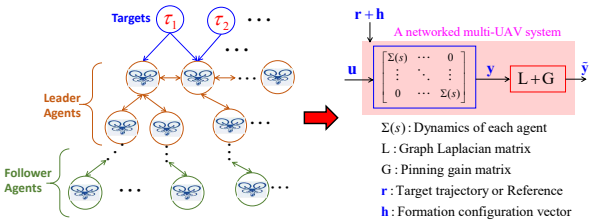

Fig. 1. Modelling of a networked multi-UAV system consisting of the leader and follower agents in a multi-agent framework.

Motivated by the recent developments in the NI-based cooperative control and its existing limitations, this paper has proposed a distributed dynamic output feedback Formation Tracking and Containment Control (FTCC) scheme for a class of MAS that can be modelled as a networked double integrator system (e.g. a group of UAVs, UGVs, two-wheeled mobile robots, etc.) exploiting Strictly Negative Imaginary Systems (SNI) property. Compared to the existing techniques, the new FTCC scheme i) considers different roles of the agents (i.e. the leader and follower agents); ii) uses only output information of the neighbouring agents; therefore, it is more useful when full-state feedback is unavailable; iii) offers greater flexibility in selecting a controller transfer function resulting in better FTCC performance; iv) is proven by exploiting the characteristic loci property of networked NI and SNI systems instead of the Lyapunov stability approach; therefore, it simplifies the stability analysis since it is not required to search for Lyapunov candidate functions; and v) offers a fault-tolerance property against a sudden loss of agents. Finally, we conducted a real-time flight experiment on a group of networked Crazyflie quadcopters to validate the proposed FTCC scheme and its fault-tolerance property.

II. Preliminaries and Problem Formulation

A. NI and SNI nomenclature

This subsection includes the frequency-domain definitions of NI and SNI systems.

This work was supported by the Engineering and Physical Sciences Research Council (EPSRC) [grant number EP/R008876/1] and the Science and Engineering Research Board (SERB), DST, India [grant number SRG/2022/000892]. All research data supporting this publication are directly available within this publication. For the purpose of open access, the authors have applied a Creative Commons Attribution (CC BY) licence to any Author Accepted Manuscript version arising.

Y.-H. Su and A. Lanzon are with the Department of EEE, School of Engineering, University of Manchester, Manchester M13 9PL, UK, and P. Bhowmick is with the Department of EEE, IIT Guwahati, Assam - 781039, India. Emails: Yu-Hsiang.Su@manchester.ac.uk, parijat.bhowmick@iitg.ac.in, Alexander.Lanzon@manchester.ac.uk.

Definition 1: (**NI Systems**) [3], [19] A system $\Sigma(s) \in \mathscr{R}^{m\times m}$ is NI if: (a) it has no RHP poles, (b) $j[\Sigma(j\omega) - \Sigma(j\omega)^*] \geq 0\ \forall\omega \in (0,\infty)$ except those $\omega_0 \in (0,\infty)$ where $s = j\omega_0$ is a pole of $\Sigma(s)$, (c) if $\omega_0 \in (0,\infty)$ is such that $s = j\omega_0$ is a pole, then the multiplicity of the pole must be one and the residue matrix $\lim_{s\to j\omega_0}(s - j\omega_0)j\Sigma(s) \geq 0$, (d) if $s = 0$ is a pole of $\Sigma(s)$, then the multiplicity of the pole at $s = 0$ cannot be more than two and the residue matrix $\lim_{s\to 0} s^2\Sigma(s) \geq 0$.

Definition 2: (**SNI Systems**) [1], [3] A system $\Sigma(s) \in \mathscr{RH}_\infty^{m\times m}$ is SNI if $j[\Sigma(j\omega) - \Sigma(j\omega)^*] > 0\ \forall\omega \in (0,\infty)$.

B. Graph theory

In this work, we use a weighted undirected graph $\mathscr{G} = \{\mathscr{V}, \mathscr{E}, \mathscr{A}\}$ to represent the interaction topology among networked agents, where $\mathscr{V} = \{1, ..., N\}$, $\mathscr{E} \subset \mathscr{V} \times \mathscr{V}$ and $\mathscr{A} = [a_{ij}] \in \mathbb{R}^{N\times N}$ are the node set, the edge set and the adjacency matrix respectively. The edge $e_{ji} = (v_j, v_i) \in \mathscr{E}$ denotes the information passes from node j to node i. We also define $\mathscr{N}_i = \{v_j | (v_j, v_i) \in \mathscr{E}\}$ as the set of all neighbours of node i. a_{ij} represents the weight of e_{ji} and $a_{ij} > 0$ if $e_{ji} \in \mathscr{E}$. The in-degree matrix is defined as $\mathscr{D} = \text{diag}\{d_i\} \in \mathbb{R}^{N\times N}$ with $d_i = \sum_{j=1}^{N} a_{ij}$. The Laplacian matrix $\mathscr{L} \in \mathbb{R}^{N\times N}$ of $\mathscr{G}$ is defined as $\mathscr{L} = \mathscr{D} - \mathscr{A}$. If the i^{th} agent is connected to the target (labelled as '0'), an edge e_{0i} is said to exist between them with a pinning gain $g_i > 0$. $\mathbb{G} = \text{diag}\{g_1, g_2, \cdots, g_N\} > 0$ is a pinning-gain matrix.

C. Multi-agent NI and SNI systems

This paper exploits multi-agent NI theory for modelling and controlling a multi-UAV system whose translational dynamics after closing the loop with attitude PID controllers can be approximated as a networked decoupled three-input-three-output double integrator system (as depicted in Fig. 1) that automatically exhibit the NI property.

We will now review some fundamental properties of multi-agent NI systems. [6] first established that a homogeneous network of NI (or SNI) agents, given by $\bar{\Sigma}(s) = (\mathscr{L} + \mathbb{G}) \otimes \Sigma(s)$, retains the NI (or SNI) property and $\bar{\Sigma}(0) > 0$ (or < 0) $\Leftrightarrow \Sigma(0) > 0$ (or < 0). Recently, [8] and [9] have derived an important property of a multi-agent NI system exploiting the results of [20]. It shows that all the characteristic loci $\lambda_i(j\omega)$ of a homogeneous multi-agent NI (or SNI) system lie in the union of the third and fourth quadrants of the complex plane (also known as the characteristic loci plane, discussed in Subsection II-D). The following mathematical notation will be adopted: the phase angle contribution of each of the characteristic loci, denoted by $\phi_i(\lambda_i(j\omega))$, lies in the range $[-\pi, 0]\ \forall\omega \geq 0$ (for *NI* systems) and respectively in the range $(-\pi, 0)\ \forall\omega \in (0,\infty)$ (for *SNI* systems). This resembles the Nyquist interpretation of SISO NI and SNI transfer functions.

D. Characteristic loci theory

The concept of *characteristic loci* and its application in determining the closed-loop asymptotic stability of LTI MIMO systems were first introduced in [21] and [22]. This concept is analogous to a *multi-loop* Nyquist criterion that offers a simple graphical stability analysis tool for MIMO systems. The characteristic loci $\lambda_i(s)$, where $i \in \{1, 2, \ldots, m\}$, of any square LTI system $\Sigma(s) \in \mathscr{R}^{m\times m}$ is a conformal mapping of the complex function $\det[\Sigma(s)]$ into another complex plane when s follows the standard s-plane D-contour in a clockwise (CW) direction (see Fig. 3a).

Theorem 1: [21], [22] A necessary and sufficient criterion for a closed-loop interconnection of two LTI systems $\Sigma(s)$ and $\Sigma_c(s)$, connected via a negative feedback, to maintain the asymptotic stability is that the total number of counter-clockwise (CCW) encirclements about the $(-1 + j0)$ point by the characteristic loci $\lambda_i(j\omega)$ of $L(s) = \Sigma(s)\Sigma_c(s)\ \forall i \in \{1, 2, \ldots, p\}$ should be equal to the number of RHP poles of $L(s)$. When $L(s) \in \mathscr{RH}_\infty^{p\times p}$, none of the characteristic loci $\lambda_i(j\omega)$ should encircle the $(-1 + j0)$ point.

E. Problem formulation

Given a multi-agent NI system, the control problem is to design an NI-based Formation Tracking and Containment Control (FTCC) scheme such that: (i) leader agents attain a prescribed formation; (ii) follower agents achieve containment by converging into a safe area guarded by the leaders (i.e. the convex hull spanned by the leaders); and (iii) the objectives mentioned in (i) and (ii) should withstand the situation of a sudden loss of agents.

III. An NI-based Formation Tracking and Containment Control Scheme

This section describes the key contributions of this paper. A distributed dynamic output feedback formation tracking and containment control scheme is derived for a class of MAS whose dynamics/kinematics can be approximated by networked double integrator agents ($\frac{1}{s^2}$). NI systems theory is utilised to design this control scheme.

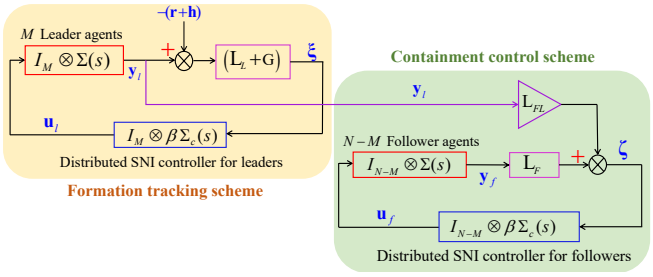

Fig. 2. A formation tracking and containment control scheme for a networked multi-UAV system involving distributed SNI controllers.

We consider a team of N networked UAVs, consisting of M leader agents and $N-M$ follower agents. The closed-loop translational dynamics of the UAVs can be approximated by a decoupled three-input-three-output double integrator system ($\frac{1}{s^2} I_3$) that inherently exhibit the NI property with a double pole at $s = 0$. The readers are referred to Subsection V-A for details. This fact inspires us to apply NI theory to develop a distributed dynamic output feedback FTCC scheme for MAS (aiming at applications to multi-UAV systems). In this work, the graph Laplacian matrix of the overall

interaction topology can be expressed in the partitioned form as $\mathscr{L} = \left[\begin{array}{c|c} \mathscr{L}_L & 0 \\ \hline \mathscr{L}_{FL} & \mathscr{L}_F \end{array}\right]$ where $\mathscr{L}_L \in \mathbb{R}^{M\times M}$, $\mathscr{L}_F \in \mathbb{R}^{(N-M)\times(N-M)}$ and $\mathscr{L}_{FL} \in \mathbb{R}^{(N-M)\times M}$. We will now mention some properties regarding the interaction topology $\mathscr{G}$ of the networked MAS.

Property 1: For an undirected graph topology, the leader must be well-connected. At least one leader must be directly connected to the target (treated as the root node labelled with $\tau_1, \tau_2, \cdots$ in Fig. 1). For a directed graph, there must exist a spanning tree from the target.

Property 2: The followers must be well-connected and at least, one leader must exist for each follower that has a directed path to that follower. The leaders only receive information from the target and/or other leaders.

As a result of Property 1, for an undirected graph, $(\mathscr{L}_L + \mathbb{G}) > 0$. Because of Property 2, all the rows of the matrix $-\mathscr{L}_F^{-1}\mathscr{L}_{FL}$ result in a row-sum equal to 1. This is a useful result from matrix theory related to algebraic graphs [23]. We are now ready to derive the main theorem of this paper, which is an NI-based FTCC scheme for MAS.

Theorem 2: Given a team of N networked MAS, consisting of M leaders and $N-M$ followers, whose closed-loop translational dynamics (in each channel) can be approximated by $\Sigma(s) = \frac{1}{s^2}$. Suppose the interaction topology $\mathscr{G}$ satisfies Properties 1 and 2. Choose an *SNI controller* $\Sigma_c(s)$ with $\Sigma_c(0) < 0$ for the scheme shown in Fig. 2. Let $\mathbf{r} = \mathbf{1}_M r$ denote the position of the target and $\mathbf{h} = [h_1, h_2, \cdots, h_M]^\top$ denote the desired formation configuration vector for leader agents. Then, the network of linearised double integrator agents achieves formation tracking and containment objectives by the following distributed dynamic output feedback SNI control law

$$u_i = \beta\Sigma_c(s)\sum_{j\in\mathscr{N}_i} a_{ij}\big((y_i - h_i) - (y_j - h_j)\big) + g_i(y_i - h_i - r) \qquad \forall i \in \{1,2,\ldots,M\} \quad (1)$$

$$\text{and } u_k = \beta\Sigma_c(s)\sum_{j\in\mathscr{N}_k} a_{kj}\big(y_k - y_j\big) \qquad \forall k \in \{M+1, M+2, \ldots, N\} \quad (2)$$

for any $\beta \in (0,\infty)$.

Proof. We have divided the proof into two parts: Part I takes care of the formation tracking of the leaders, and Part II establishes containment control of the followers.

Part I: Formation tracking of the leader agents

The closed-loop control scheme shown at the top of Fig. 2 is responsible for formation tracking, which has the loop transfer function $T_L = (\mathscr{L}_L + \mathbb{G}) \otimes \frac{1}{s^2}\Sigma_c(s)$. The symbol $\bar{\lambda}_i(s)$ represents the characteristic loci of T_L where $i \in \{1,2,\ldots,M\}$. To proceed with the proof, three sets Ψ_0, $\Psi_{\pm\Im}$ and Ψ_∞ of the Laplace variable s are defined corresponding to three specific regions marked along the standard s-plane D-contour (as shown in Fig. 3a). To prove the asymptotic stability of the proposed formation control scheme, we will exploit the characteristic loci theorem (Theorem 1). This proof consists of the following three cases. In

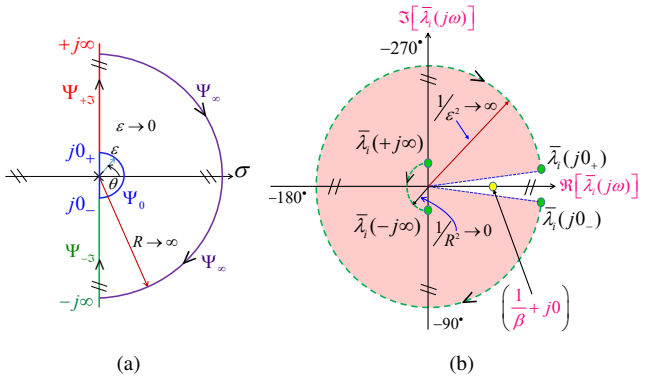

(a) (b)

Fig. 3. (a) The standard s-plane Nyquist $\mathscr{D}$-contour; and (b) All the characteristic loci $\bar{\lambda}_i(s)$ of $(\mathscr{L}_L+\mathbb{G})\otimes\frac{1}{s^2}\Sigma_c(s)$ lie inside the Red-coloured region when $\Sigma_c(s)$ is SNI with $\Sigma_c(0) < 0$.

Part I, the index $i \in \{1,2,\ldots,M\}$ will be used uniformly for the leader agents.

Case I: For the subset $s \in \Psi_0$

We can approximately express the characteristic loci $\bar{\lambda}_i(s)$

$$\bar{\lambda}_i(s)|_{s\in\Psi_0} = \lambda_i\left[(\mathscr{L}_L + \mathbb{G}) \otimes \Sigma_c(0)\right]\frac{1}{\varepsilon^2}e^{-j2\theta} \quad (3)$$

where λ_i simply denotes the i^{th} eigenvalue of a real matrix. Let $\lambda_i\left[(\mathscr{L}_L + \mathbb{G}) \otimes \Sigma_c(0)\right] = c_i e^{j\phi_i}$ where $\phi_i = -\pi\ \forall i$ since $\Sigma_c(0) < 0$ and $(\mathscr{L}_L + \mathbb{G}) > 0$. Then, (3) takes the form $\bar{\lambda}_i(s)|_{s\in\Psi_0} = \frac{c_i}{\varepsilon^2}e^{j(\phi_i - 2\theta)}$. Therefore, $\bar{\lambda}_i(j0_+) = \frac{c_i}{\varepsilon^2}e^{-j2\pi} \to +\infty\angle -2\pi$ when $\theta = \frac{\pi}{2}$ and considering $\varepsilon \to 0_+$. Similarly, $\bar{\lambda}_i(j0_-) \to +\infty\angle 0$ when $\theta = -\frac{\pi}{2}$ as the characteristic loci are symmetric about the real axis. It is essential to note here that $\angle\bar{\lambda}_i(j0_+) > -2\pi\ \forall i$ since $\angle\gamma(j0_+) > -\pi$. Similarly, $\bar{\lambda}_i(j0_-) \to +\infty\angle 0\ \forall i$ with $\angle\bar{\lambda}_i(j0_-) < 0$. This implies $-2\pi < \angle\bar{\lambda}_i(j\omega) < 0\ \forall i$ when $s \in \Omega_0$. Each locus $\bar{\lambda}_i(j\omega)$ connects the $\bar{\lambda}_i(j0_-)$ and $\bar{\lambda}_i(j0_+)$ points (computed at $\omega = 0_+$ and $\omega = 0_-$) in a CW direction through an almost circular arc having radius $\frac{1}{\varepsilon^2} \to \infty$ as depicted in Fig. 3b. The above analysis guarantees that none of the characteristic loci $\bar{\lambda}_i(j\omega)$ crosses the positive real axis at an infinite distance.

Case II: For the subset $s \in \Psi_{\pm\Im}$

We assume again $\lambda_i\left[(\mathscr{L}_L + \mathbb{G}) \otimes \Sigma_c(j\omega)\right] = c_i e^{j\phi_i}$ for all $\omega \in (0,\infty)$. Since $\Sigma_c(s)$ is SNI, $\phi_i(\omega) \in (-\pi, 0)\ \forall\omega \in (0,\infty)$ and hence, for all i, $\angle\bar{\lambda}_i(j\omega) = (\phi_i - \pi) \in (-2\pi, -\pi]\ \forall\omega \in (0,\infty)$. Following the same logic, we can assert $\angle\bar{\lambda}_i(j\omega) \in [-\pi, 0)$ when $\omega \in (-\infty, 0)$. Ultimately, we can conclude that all $\bar{\lambda}_i(j\omega)$ remain inside the Red-coloured region shown in Fig. 3b when $s \in \Psi_{\pm\Im}$. We emphasize that none of the $\bar{\lambda}_i(j\omega)$ intersects the positive real axis at finite/infinite distance.

Case III: For the subset $s \in \Psi_\infty$

Similar to Case I, for this subset also, we can write

$$\bar{\lambda}_i(s)|_{s\in\Psi_\infty} = \lambda_i\left[(\mathscr{L}_L + \mathbb{G}) \otimes \Sigma_c(\infty)\right]\frac{e^{-j2\theta}}{R^2} = \frac{c_i}{R^2}e^{j(\phi_i - 2\theta)}$$

upon letting $\lambda_i\left[(\mathscr{L}_L+\mathbb{G})\otimes\Sigma_c(\infty)\right]=c_ie^{j\phi_i}$ where λ_i denotes the eigenvalues. Note that $\phi_i=-\pi$ as $\Sigma_c(\infty)<0$ is implied by $\Sigma_c(0)<0$ and $\Sigma_c(s)$ being SNI. Therefore, $\bar{\lambda}_i(+j\infty)=\frac{c_i}{R^2}e^{j(\phi_i-\frac{\pi}{2})}\rightarrow 0\angle-\frac{3\pi}{2}$ as $R\rightarrow\infty$ and similarly, $\bar{\lambda}_i(-j\infty)\rightarrow 0\angle-\frac{\pi}{2}$. This then follows that each $\bar{\lambda}_i(j\omega)$ joins the $\bar{\lambda}_i(+j\infty)$ and $\bar{\lambda}_i(-j\infty)$ points (computed at $\omega=+\infty$ and $\omega=-\infty$) in the CCW direction via a semicircular arc of radius $\frac{1}{R^2}\rightarrow 0$ as illustrated in Fig. 3b.

The above three cases can be combined together to guarantee that all the characteristic loci $\bar{\lambda}_i(s)$ of $T_L(s)$ remain inside the Red-coloured area marked in Fig. 3b. This is equivalent to saying that for any value of β in the range $(0,\infty)$, the critical point $(\frac{1}{\beta}+j0)$ is not encircled by any characteristic loci $\bar{\lambda}_i(s)$. This proves the asymptotic stability of the proposed formation tracking scheme.

We will now establish the asymptotic convergence of the formation tracking error $\boldsymbol{\xi}=[\xi_1,\xi_2,\cdots,\xi_M]^\top$. The error dynamics can be obtained from the block diagram in Fig. 2 as $\boldsymbol{\Xi}(s)=\left[I-\left((\mathscr{L}_L+\mathbb{G})\otimes\frac{\beta}{s^2}\Sigma_c(s)\right)\right]^{-1}$. The expression of the time-domain steady-state error can be derived as

$$
\begin{aligned}
\boldsymbol{\xi}_{ss}&=\lim_{t\rightarrow\infty}\boldsymbol{\xi}(t)=\lim_{s\rightarrow 0}s\,\boldsymbol{\Xi}(s)\\
&=\lim_{s\rightarrow 0}s\left[I-\left((\mathscr{L}_L+\mathbb{G})\otimes\frac{\beta}{s^2}\Sigma_c(s)\right)\right]^{-1}\hat{\mathbf{R}}(s)\\
&\qquad[\text{denoting }\hat{\mathbf{r}}=-(\mathbf{r}+\mathbf{h})\text{ and }\hat{\mathbf{R}}(s)=\text{Laplace of }\hat{\mathbf{r}}]\\
&=\lim_{s\rightarrow 0}s^2\left[s^2I-\left((\mathscr{L}_L+\mathbb{G})\otimes\beta\Sigma_c(s)\right)\right]^{-1}(s\hat{\mathbf{R}}(s))\\
&=-\left[(\mathscr{L}_L+\mathbb{G})\otimes\beta\Sigma_c(0)\right]^{-1}\left(\lim_{s\rightarrow 0}s^2I\right)\times\\
&\qquad\left(-\lim_{s\rightarrow 0}s\big[\mathbf{R}(s)+\mathbf{H}(s)\big]\right)=[0,0,\cdots,0]^\top
\end{aligned}
$$

since $\Sigma_c(0)<0$, $(\mathscr{L}_L+\mathbb{G})>0$ and $\mathbf{r}(t)$ and $\mathbf{h}(t)$ all are bounded signals for all $t\geq 0$. This hence implies $\mathbf{y}\rightarrow-\hat{\mathbf{r}}\rightarrow(\mathbf{r}+\mathbf{h})$ at the steady-state.

The same proof can be easily extended to all three channels taken together, i.e., when $\Sigma(s)=\frac{1}{s^2}I_3$ and accordingly, $u_i\in\mathbb{R}^3$, $y_i\in\mathbb{R}^3$, $\xi_i\in\mathbb{R}^3$, $h_i\in\mathbb{R}^3$ and $r=[r_x,r_y,r_z]^\top$. For which, the controller becomes $\Sigma_c(s)I_3$. The Kronecker product form will then be used in all expressions.

Part II: Containment control of the follower agents

Following the same procedure as in Part I, the asymptotic stability of the containment control scheme (the lower block diagram in Fig. 2) for the followers can be readily established along with $\lim_{t\rightarrow\infty}\boldsymbol{\zeta}(t)=0$ where $\boldsymbol{\zeta}$ denotes the containment error. This implies $\lim_{t\rightarrow\infty}\left(\mathscr{L}_F\,\mathbf{y}_f+\mathscr{L}_{FL}\,\mathbf{y}_l\right)=0\Leftrightarrow\lim_{t\rightarrow\infty}\left(\mathbf{y}_f+\mathscr{L}_F^{-1}\mathscr{L}_{FL}\,\mathbf{y}_l\right)=0\Leftrightarrow\lim_{t\rightarrow\infty}\left(y_k-\sum_{j=1}^{M}\alpha_{kj}y_j\right)=0$ for all $k\in\{M+1,M+2,\ldots,N\}$ where $\mathbf{y}_l=[y_1,y_2,\cdots,y_M]^\top$, $\mathbf{y}_f=[y_{(M+1)},y_{(M+2)},\cdots,y_N]^\top$ and $\sum_{j=1}^{M}\alpha_{kj}=1$ with $\alpha_{kj}>0$ since each row sum of the matrix $-\mathscr{L}_F^{-1}\mathscr{L}_{FL}$ is equal to 1. This means that all followers will be driven inside a convex hull spanned by the coordinates of the leaders [24]. This completes the proof. ■

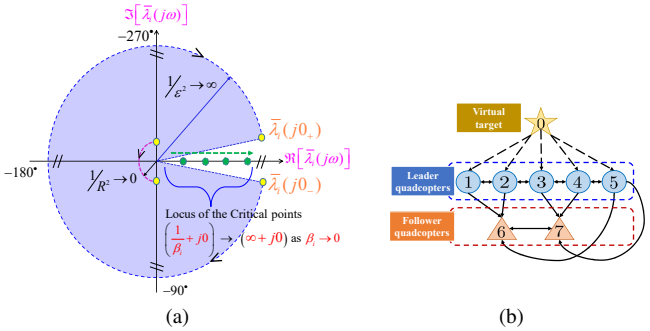

Fig. 4. (a) None of the characteristic loci $\bar{\lambda}_i(j\omega)$ of $[(\mathscr{L}+\mathbb{G})\otimes\frac{1}{s^2}\Sigma_c(s)]$ encircles any of the critical points $(\frac{1}{\beta_i}+j0)$ when β_i varies in the range $[0,\infty)$; and (b) The interaction topology among networked quadcopter UAVs (both leader and follower agents) and the virtual target considered in the flight experiment in Subsection V-B.

IV. Fault-tolerance property

When designing controllers for networked MAS, we often encounter difficulties due to a sudden loss of agents caused either by hardware faults or communication failure. Preservation of the stability of a MAS upon the loss of some agents is of utmost interest. That is, subject to a sudden loss of agents, the cooperative control scheme should be able to maintain the overall stability of the network. Also, a new stable operating condition should be reached via an autonomous reconfiguration of the network topology, i.e., after excluding the faulty agents. Motivated by the ideas of [8] and [9] (which were built on the results of [20]), we will now show that the proposed NI-based FTCC scheme has a fault-tolerance property. The case of a loss of one/multiple agent(s) can be theoretically considered by making the gain(s) of that particular control loop goes to zero (i.e. $\beta_i=0$), which means that the faulty loop is temporarily deactivated. The lemma below will show that the proposed NI-based FTCC scheme is able to maintain the overall stability in the case of a sudden loss of agents.

Lemma 1: Under the assumptions of Theorem 2, the FTCC law given by (1) and (2) preserves the asymptotic stability of the overall closed-loop system in Fig. 2 when one/multiple agent(s) suddenly stops working and leaves the network.

Proof. Theorem 2 has established the closed-loop stability of both the formation tracking and containment control schemes (shown in a coupled configuration in Fig. 2) for a MAS whose closed-loop translational dynamics can be approximated by a double integrator system for any $\beta\in(0,\infty)$. This was established by showing that none of the characteristic loci $\bar{\lambda}_i(s)$ of $\left[(\mathscr{L}+\mathbb{G})\otimes\frac{1}{s^2}\Sigma_c(s)\right]$ encircles the critical point $(\frac{1}{\beta_i}+j0)$ for any $\beta_i\in(0,\infty)$. When $\beta_i\rightarrow 0$, the corresponding critical point $(\frac{1}{\beta_i}+j0)$ approaches $(\infty+j0)$, as portrayed in Fig. 4a. The loss of an agent is taken into account by making $\beta_i=0$, which causes the critical point to reach $(\infty+j0)$. Fortunately, as observed in Fig. 4a, all $\bar{\lambda}_i(s)$ remain inside the Purple-coloured region and hence, there is no possibility of intersecting the positive real axis anywhere by any characteristic locus. This ensures

that even when the critical point lies at $(\infty + j0)$ conforming with $\beta_i = 0$, it will not be encircled by any $\bar{\lambda}_i(s)$. This, in turn, implies that the closed-loop stability remains preserved even when $\beta_i = 0$ [which indicates that the i^{th} agent is faulty and is excluded from the network]. The concept applies to both the formation tracking and containment control configurations. ■

V. Hardware implementation on UAVs

A real-time flight experiment was conducted on seven networked Crazyflie 2.1 nano quadcopters to validate the control performance and fault-tolerance property of the proposed NI-based FTCC scheme. A Loco Positioning system (LPS) is used to detect the positions of each quadcopter with an accuracy of $0.1\,\text{m}$ [25]. The position information of each quadcopter is transmitted to a base station, and the control command is generated through the base station and sent to each quadcopter via Crazyradio dongles [25]. However, since the proposed control strategy is completely distributed, the base station can be removed if the quadcopters can sense their relative positions w.r.t. its neighbours or directly exchange their position information via Bluetooth or Wi-Fi. A recorded video clip of the real-time flight experiment can be found at `https://youtu.be/5wD7zETI670`.

A. Modelling of quadcopter UAVs

Let $\mathbf{p} = [p_x, p_y, p_z]^\top$, $\boldsymbol{\omega} = [p, q, r]^\top$ and $\boldsymbol{\eta} = [\phi, \theta, \psi]^\top$ be the position vector in the earth frame, the angular velocity vector in the body frame and the Euler angles respectively. According to Newton-Euler equations, the dynamics of a small and lightweight quadcopter UAV can be represented as follows

$$\begin{cases} m\ddot{\mathbf{p}} = -mg\mathbf{e}_z + \mathbf{R}_e^b(\boldsymbol{\eta})\mathbf{F}_b, \\ \mathbf{I}\dot{\boldsymbol{\omega}} = -\boldsymbol{\omega} \times \mathbf{I}\boldsymbol{\omega} + \boldsymbol{\tau}_b, \end{cases} \tag{4}$$

where $m \in \mathbb{R}$ and $\mathbf{I} \in \mathbb{R}^{3\times 3}$ are the mass and the inertia matrix of a quadcopter UAV, g is the gravity constant, $\mathbf{e}_z = [0, 0, 1]^\top$ is the unit vector w.r.t. the earth frame, $\mathbf{R}_e^b(\boldsymbol{\eta}) \in \mathbb{R}^{3\times 3}$ is the rotation matrix from the body frame to the earth frame, following the $Z \to Y \to X$ Euler rotation sequence, $\mathbf{F}_b$ is the total force (in the body frame) from the rotors and $\boldsymbol{\tau}_b$ is the total drag torque (in the body frame) produced by the rotors.

Remark 1: Since the attitude dynamics of quadcopter UAVs are much faster than the translational dynamics, flight control can be solved by a two-loop cascade control configuration (see [24] and references therein). The distributed cooperative control law in the outer-loop drives the networked quadcopters to achieve formation tracking and containment control, while the inner-loop control (a single/cascaded PID can be used) stabilises the attitude dynamics. As a result, the closed-loop translational dynamics of a quadcopter UAV can be approximated by a decoupled three-input-three-output double integrator system $\ddot{\mathbf{p}}_i = \mathbf{u}_i$, where $\mathbf{p}_i = [p_{x_i}, p_{y_i}, p_{z_i}]^\top$ and $\mathbf{u}_i = [u_{x_i}, u_{y_i}, u_{z_i}]^\top$ are the position and control input vectors of the i^{th} quadcopter UAV.

According to Remark 1, the proposed NI-based FTCC scheme in Theorem 2 can be applied in the outer-loop control to drive a multi-UAV system to achieve the desired formation tracking and containment behaviours. The output feedback $\mathbf{y}_i = \mathbf{p}_i$ is the position vector of the i^{th} quadcopter UAV and the control input vector $\mathbf{u}_i$ can be designed by the distributed dynamic output feedback SNI control law in (1) and (2).

B. Experimental validation results

In the real-time flight experiment, a three-dimensional formation tracking and containment flight mission is performed by seven networked Crazyflie quadcopters, consisting of five leader and two follower agents. Fig. 4b describes the interaction topology for the networked quadcopter UAVs and the virtual target satisfying Properties 1 and 2. In addition, we chose an *SNI controller* $\Sigma_c(s) = -\frac{s+1}{s+20}$ with $\Sigma_c(0) = -\frac{1}{20} < 0$ and $\beta = 20$ to be implemented in the hardware experiment. The experimental objectives are given below:

1) The five leader quadcopters must achieve the three-dimensional pyramid formation while the two followers must enter into the convex hull spanned by the positions of the leaders;
2) After a sudden loss of one leader quadcopter, the remaining four leaders must reconfigure into a two-dimensional diamond shape formation while the two followers must enter into the new convex hull spanned by the coordinates of the remaining four leaders.

Fig. 5 presents the snapshots of the real-time flight experiment. Fig. 5a shows the positions of all quadcopters after taking off, in which five leader quadcopters did not form the prescribed three-dimensional pyramid formation, and two followers were outside the convex hull spanned by the coordinates of the leaders. Next, Fig. 5b shows that five leader quadcopters achieved the prescribed three-dimensional pyramid formation, and two followers entered into the convex hull spanned by the coordinates of the leaders. Finally, Fig. 5c shows that after the leader quadcopter at the top experienced a sudden malfunction and dropped to the ground (i.e. marked by the yellow cross), the remaining four leader quadcopters reconfigured into a two-dimensional diamond shape formation, and two followers entered into the new convex hull spanned by the coordinates of the remaining four leaders. Fig. 6 presents the 2-norms of the formation tracking and containment errors, in which they all converge to nearly zero. The experimental results validate that seven networked quadcopters achieved the formation tracking and containment flight mission in both healthy and faulty operating conditions via the proposed NI-based FTCC scheme.

VI. Conclusions

This paper resorts to Strictly Negative Imaginary systems property to design a distributed dynamic output feedback formation tracking and containment control scheme for networked multi-UAV systems. Compared to the conventional formation-containment control schemes that use a full-state feedback approach, the proposed methodology relies only on output feedback, which is more practical when full-state

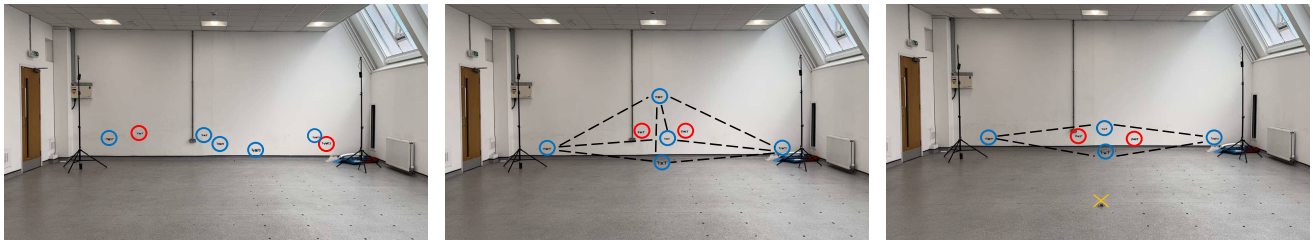

(a) $t = 0\,\mathrm{s}$ (b) $t = 15\,\mathrm{s}$ (c) $t = 25\,\mathrm{s}$

Fig. 5. Snapshots of the real-time flight experiment at $t = 0\,\mathrm{s}$, $t = 15\,\mathrm{s}$ and $t = 25\,\mathrm{s}$. The blue and red circles represent the leader and follower quadcopters. The black dashed lines mark the formations of the leader quadcopters.

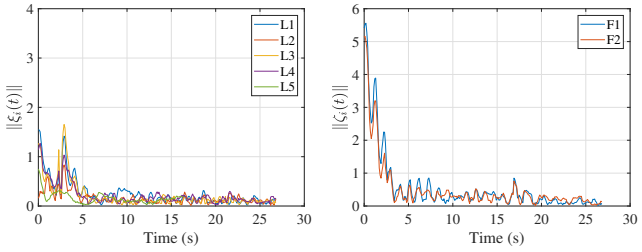

(a) Formation tracking error $\|\boldsymbol{\xi}_i(t)\|$. (b) Containment error $\|\boldsymbol{\zeta}_i(t)\|$.

Fig. 6. (a) The formation tracking error of each leader quadcopter; (b) The containment error of each follower quadcopter.

information is unavailable. Furthermore, this methodology uses the characteristic loci technique to prove the asymptotic stability of the formation and containment error dynamics instead of the commonly-used Lyapunov theory-based approach. Finally, a real-time flight experiment involving seven networked Crazyflie quadcopters was conducted to test the feasibility and performance of the proposed scheme and its fault-tolerance property to a sudden loss of agents.

REFERENCES

[1] A. Lanzon and I. R. Petersen, "Stability robustness of a feedback interconnection of systems with negative imaginary frequency response," *IEEE Transactions on Automatic Control*, vol. 53, no. 4, pp. 1042–1046, May 2008.

[2] P. Bhowmick and S. Patra, "On LTI output strictly negative-imaginary systems," *Systems & Control Letters*, vol. 100, pp. 32–42, Feb 2017.

[3] A. Lanzon and H.-J. Chen, "Feedback stability of negative imaginary systems," *IEEE Transactions on Automatic Control*, vol. 62, no. 11, pp. 5620–5633, Nov 2017.

[4] S. Kurawa, P. Bhowmick, and A. Lanzon, "Dynamic output feedback controller synthesis using an LMI-based α-strictly negative imaginary framework," in *Proceedings of 27th Mediterranean Conference on Control and Automation*, July 2019, pp. 81–86.

[5] L. Liu and G. Wu, "Active vibration suppression and precision pointing control of piezo-based platforms and their applications to flexible spacecrafts," in *Proceedings of the 10th IEEE International Conference on Control and Automation*, June 2013, pp. 890–895.

[6] J. Wang, A. Lanzon, and I. R. Petersen, "Robust output feedback consensus for networked negative-imaginary systems," *IEEE Transactions on Automatic Control*, vol. 60, no. 9, pp. 2547–2552, Sep 2015.

[7] O. Skeik, J. Hu, F. Arvin, and A. Lanzon, "Cooperative control of integrator negative imaginary systems with application to rendezvous multiple mobile robots," in *Proceedings of 12th International Workshop on Robot Motion and Control*, July 2019, pp. 15–20.

[8] J. Hu, B. Lennox, and F. Arvin, "Robust formation control for networked robotic systems using negative imaginary dynamics," *Automatica*, vol. 140, no. 110235, pp. 1–9, June 2022.

[9] P. Bhowmick, A. Ganguly, and S. Sen, "A new consensus-based formation tracking scheme for a class of robotic systems using negative imaginary property," *IFAC-PapersOnLine*, vol. 55, no. 1, pp. 685–690, 2022.

[10] V. P. Tran, M. A. Garratt, and I. R. Petersen, "Multi-vehicle formation control and obstacle avoidance using negative-imaginary systems theory," *IFAC Journal of Systems and Control*, vol. 15, no. 100117, pp. 1–23, March 2021.

[11] C. Li, J. Wang, J. Shan, A. Lanzon, and I. R. Petersen, "Robust cooperative control of networked train platoons: A negative-imaginary systems' perspective," *IEEE Transactions on Control of Network Systems*, vol. 8, no. 4, pp. 1743–1753, Dec 2021.

[12] P. Bhowmick and A. Lanzon, "Output strictly negative imaginary systems and its connections to dissipativity theory," in *Proceedings of 58th IEEE Conference on Decision and Control*, Dec 2019, pp. 6754–6759.

[13] ——, "Time-domain output negative imaginary systems and its connection to dynamic dissipativity," in *Proceedings of 59th IEEE Conference on Decision and Control*, Dec 2020, pp. 5167–5172.

[14] S. Kurawa, P. Bhowmick, and A. Lanzon, "Negative imaginary theory for a class of linear time-varying systems," *IEEE Control Systems Letters*, vol. 5, no. 3, pp. 1001–1006, 2021.

[15] A. Lanzon and P. Bhowmick, "Characterisation of input-output negative imaginary systems in a dissipative framework," *IEEE Transactions on Automatic Control*, vol. 68, no. 2, pp. 959–974, Feb 2023.

[16] Z. Li and Z. Duan, *Cooperative Control of Multi-Agent Systems : A Consensus Region Approach*, ser. Automation and Control Engineering. Bosa Roca: CRC Press, 2014.

[17] W. Ren, R. W. Beard, and E. M. Atkins, "Information consensus in multivehicle cooperative control," *IEEE Control Systems Magazine*, vol. 27, no. 2, pp. 71–82, April 2007.

[18] H. Liu, L. Cheng, M. Tan, Z. Hou, Z. Cao, and M. Wang, "Containment control with multiple interacting leaders under switching topologies," in *Proceedings of the 32nd Chinese Control Conference*, Xian, China, 2013, pp. 7093–7098.

[19] M. A. Mabrok, A. G. Kallapur, I. R. Petersen, and A. Lanzon, "Generalizing negative imaginary systems theory to include free body dynamics: Control of highly resonant structures with free body motion," *IEEE Transactions on Automatic Control*, vol. 59, no. 10, pp. 2692–2707, Oct 2014.

[20] P. Bhowmick and S. Patra, "On decentralized integral controllability of stable negative-imaginary systems and some related extensions," *Automatica*, vol. 94, pp. 443–451, Aug 2018.

[21] J. J. Belletrutti and A. G. J. MacFarlane, "Characteristic loci techniques in multivariable-control-system design," *Proceedings of the Institution of Electrical Engineers*, vol. 118, no. 9, pp. 1291–1297, Sep 1971.

[22] A. G. J. Macfarlane and J. J. Belletrutti, "The characteristic locus design method," *Automatica*, vol. 9, no. 5, pp. 575–588, 1973.

[23] Z. Li and Z. Duan, *Cooperative control of multi-agent systems: A consensus region approach*, 1st ed. CRC Press, 2014.

[24] Y.-H. Su and A. Lanzon, "Formation-containment tracking and scaling for multiple quadcopters with an application to choke-point navigation," in *Proceedings of the IEEE International Conference on Robotics and Automation*, May 2022, pp. 4908–4914.

[25] Bitcraze, "https://www.bitcraze.io."